

Constraining Intermediate-Mass Black Holes in Globular Clusters

Stefan Umbreit

Center for Interdisciplinary Exploration and Research in Astrophysics (CIERA) & Dept. of
Physics and Astronomy, Northwestern University, 2145 Sheridan Rd, Evanston, IL 60208,
USA

`s-umbreit@northwestern.edu`

and

Frederic A. Rasio

Center for Interdisciplinary Exploration and Research in Astrophysics (CIERA) & Dept. of
Physics and Astronomy, Northwestern University, 2145 Sheridan Rd, Evanston, IL 60208,
USA

`rasio@northwestern.edu`

Received _____; accepted _____

Abstract

Decades after the first predictions of intermediate-mass black holes (IMBHs) in globular clusters (GCs) there is still no unambiguous observational evidence for their existence. The most promising signatures for IMBHs are found in the cores of GCs, where the evidence now comes from the stellar velocity distribution, the surface density profile, and, for very deep observations, the mass-segregation profile near the cluster center. However, interpretation of the data, and, in particular, constraints on central IMBH masses, require the use of detailed cluster dynamical models. Here we present results from Monte Carlo cluster simulations of GCs that harbor IMBHs. As an example of application, we compare velocity dispersion, surface brightness and mass-segregation profiles with observations of the GC M10, and constrain the mass of a possible central IMBH in this cluster. We find that, although M10 does not seem to possess a cuspy surface density profile, the presence of an IMBH with a mass up to 0.75% of the total cluster mass, corresponding to about $600 M_{\odot}$, cannot be excluded. This is also in agreement with the surface brightness profile, although we find it to be less constraining, as it is dominated by the light of giants, causing it to fluctuate significantly. We also find that the mass-segregation profile cannot be used to discriminate between models with and without IMBH. The reason is that M10 is not yet dynamically evolved enough for the quenching of mass segregation to take effect. Finally, detecting a velocity dispersion cusp in clusters with central densities as low as in M10 is extremely challenging, and has to rely on only 20 – 40 bright stars. It is only when stars with masses down to $0.3 M_{\odot}$ are included that the velocity cusp is sampled close enough to the IMBH for a significant increase above the core velocity dispersion to become detectable.

Subject headings: black hole physics – globular clusters: general – globular clusters:
individual (NGC 6254) – methods: numerical – stars: kinematics and dynamics

1. Introduction

It has been known for a long time that cusps in the velocity dispersion or density profiles could provide strong indication for the presence of an intermediate-mass black hole (IMBH) at the center of a star cluster (see, e.g., Umbreit et al. 2012, for a short review). The existence of these black holes, with masses intermediate between stellar ($M_{BH} \lesssim 20M_{\odot}$), and supermassive ($M_{BH} \gtrsim 10^6 M_{\odot}$), could not be established by observations up until recently, although IMBHs were discussed by theorists already more than 30 years ago (see, e.g., Wyller 1970). In contrast to indirect evidence from, e.g., so-called ultra-luminous X-ray sources (ULXs), sources with luminosities that exceed what can be produced by a stellar mass BH accreting at the Eddington limit, measurements of the cusp slopes allow a more direct determination of the mass of an IMBH.

However, such cusps might not be easily detectable in real star clusters. On the one hand, cusps in the surface brightness profile (SBP) are expected to be rather shallow, making them difficult to distinguish from standard King models (Baumgardt et al. 2005). On the other hand, measurements of cusps in velocity dispersion profiles, though steeper, have to rely on only a relatively small number of stars for typical globular clusters (Baumgardt et al. 2004a). This especially applies to the old Milky Way globular clusters (hereafter GCs), where the cluster centers are most likely dominated by dark stellar remnants, reducing the number of observable bright stars in the cusp. Based on SBP measurements by Noyola & Gebhardt (2006), 9 candidate GCs with inner SBP power-law slopes in the range -0.1 to -0.3 , indicative of an IMBH, have been identified so far (Baumgardt et al. 2005). These slopes represent, however, only tentative evidence as their error bars, based on photometric and statistical errors, are rather large, ranging from 50-100% of the slope value. In addition, from N -body and Monte Carlo simulations it has been found that these slopes are rather time variable such that, e.g., the inner SBP of a cluster with IMBH could even

be completely flat for some brief period of time (Umbreit et al. 2012; Noyola & Baumgardt 2011; Vesperini & Trenti 2010; Trenti et al. 2010).

Another measure for the mass of an IMBH comes from the size of the cluster core, with more massive IMBHs producing larger cores as measured by the core-to-half light ratio (e.g., Heggie et al. 2007; Marchant & Shapiro 1980; Shapiro 1977). As shown by Miocchi (2007), the size of the core is related to the inner SBP cusp slope such that clusters with larger slopes have also lower concentrations if they contain an IMBH in their center. Thus, the structure of GCs together with their inner SBP slopes should in principle have the potential to lead to stronger constraints by placing upper *and* lower limits on the IMBH mass. Based on literature values for the inner slopes and concentrations, there are 2 clusters (from the previous list of 9 IMBH candidate clusters of Baumgardt et al. (2005)) whose concentrations are inconsistent with their inner SBP slopes, leaving 7 IMBH cluster candidates. However, as with the inner slopes of the SBP, the determination of the concentration is plagued with considerable uncertainties. This is mainly because the escape of unbound stars is delayed (Fukushige & Heggie 2000), and thus the escaping stars may contribute significantly to the outer cluster light. The escaping stars, if not considered, can lead to a much larger apparent tidal cut-off radius, and, thus, to a significantly larger estimate of the concentration parameter (Trenti et al. 2010). For instance, in Umbreit et al. (2012), we have shown that, although the concentration of the cluster NGC 5694, quoted as 1.8 in the Harris catalog, is too large for the inner SBP slope of -0.19 , it is nevertheless still consistent with the presence of an IMBH if the flattening of the outer SBP can be attributed to the stellar background.

A less sensitive measure of the mass, but more sensitive to the *presence* of an IMBH, recently proposed by Gill et al. (2008), is based on the average mass profile of main-sequence stars normalized to its value at the half-mass radius. Their direct N -body simulations show

that an IMBH changes the mass-segregation profile of the cluster such that it effectively counterbalances the tendency of massive stars to concentrate towards the center, similar to what has been reported earlier by Baumgardt et al. (2004b). Both Baumgardt et al. (2004b) and Gill et al. (2008) suggest that the reason for the so-called “quenching” of mass segregation is strong binary interactions between the massive stars sinking towards the center and any companion stars bound to the IMBH. Furthermore, a similar mechanism might be responsible for the somewhat weaker quenching of mass segregation in clusters with primordial binaries as in both cases strong binary interactions are involved.

The mass segregation signature does, however, require that the cluster has had enough time to settle down to a dynamically relaxed state, which happens over several half-mass relaxation times. Indeed, many old Milky Way GCs might be in such a relaxed state, as their estimated half-mass relaxation times are an order of magnitude shorter than their age (e.g., McLaughlin & van der Marel 2005). As shown in many studies, relaxed stellar systems evolve towards a self-similar configuration, and the cluster structure is then mostly determined by heating processes in the cluster core, such as interactions with primordial binaries (Fregeau et al. 2003; Fregeau & Rasio 2007), or with an IMBH (Baumgardt et al. 2004b, 2005; Heggie et al. 2007; Trenti et al. 2007), the formation of three-body binaries (Bettwieser & Sugimoto 1984), and stellar collisions (Chatterjee et al. 2008). From a modeling perspective, this has the advantage that the parameter space of initial cluster conditions to explore for a given observed GC is greatly reduced, as the structure of relaxed stellar systems is rather independent from the conditions at the time of their formation.

However, Umbreit et al. (2012) demonstrate that dynamic age estimates based only on the current state of clusters are very unreliable, for two reasons. First, the half-mass relaxation time is generally time dependent, so there is a dependence of the dynamic age on the previous evolutionary history of the cluster (see also Hurley 2007). Second, given a

final state, the dynamic age can differ significantly depending on the initial cluster size with respect to the tidal boundary. For instance, when a cluster significantly underfills its Roche lobe it expands freely, increasing its relaxation time, whereas for tidally filling clusters the relaxation time can decrease as the cluster cannot expand beyond the tidal radius while its core is contracting (see, e.g., Hurley 2007). As an added difficulty, it may be hard to decide in which of these categories the evolution of a particular observed cluster falls, as the tidal field the cluster experienced may have been strongly time-dependent and could require extensive analysis to constrain (e.g., Kruijssen et al. 2011; Allen et al. 2006). As a consequence of the uncertainties in the dynamic age estimates, it is not clear *a priori* whether a cluster is in the fully relaxed state or, possibly, still in its core contraction phase, which may have consequences for the observability of IMBH signatures.

From this discussion it becomes clear that meaningful constraints on the mass of a possible IMBH at the center of an observed GC require extensive analysis of detailed, realistic evolutionary cluster models, which are then compared to observations. In this paper we extend our analysis in Umbreit et al. (2012) and consider, in addition to the SBP, kinematic and mass segregation signatures. As an example of direct comparison to observations we focus on the cluster M10 (NGC 6254). This cluster is especially suited for such a comparison given its close proximity to the sun (≈ 4 kpc) and multitude of available observational data (Noyola & Gebhardt 2006; Beccari et al. 2010; Dalessandro et al. 2011). In addition to considering more observables, we now also consider clusters that fill their Roche lobes and are significantly influenced by tidal stripping.

Our paper is organized as follows. In Section 2 we briefly present the cluster Monte Carlo method, and describe initial conditions for the simulations and observations of M10. In Section 3 we present surface density, surface brightness, average mass profile, and velocity dispersion profiles from our models with and without central IMBH, and determine the

maximum mass a hypothetical IMBH could possess to be still compatible with observations. We conclude in Section 4.

2. Initial Conditions and Observations

2.1. Initial Conditions

We carried out a large parameter study to model GCs with and without IMBH using our Cluster Monte Carlo code (CMC; Umbreit et al. 2012; Chatterjee et al. 2010; Fregeau & Rasio 2007; Fregeau et al. 2003; Joshi et al. 2001, 2000). As with direct N -body codes (e.g., Aarseth 2003; Portegies Zwart et al. 2001), CMC uses a star-by-star, discrete representation of the cluster, and the code is now able to treat all relevant processes such as stellar evolution (Chatterjee et al. 2010), strong interactions between stars and binaries (Fregeau & Rasio 2007), as well as the dynamics of a central massive BH, including an advanced treatment of the loss cone physics needed to accurately estimate the rate of cluster heating (Umbreit et al. 2012). The dynamical evolution of the cluster is computed on the relaxation timescale (i.e., the timestep is a fraction of the relaxation time, $\sim 10^9$ yr for a typical GC, rather than the much shorter dynamical time, $\sim 10^6$ yr) which enables us to calculate the evolution of massive GCs in a relatively short time (typically less than a week on a modern workstation).

Our study consists of approximately 500 model calculations varying IMBH mass, initial number of stars, cluster concentration, and distance from the Galactic center. The positions and velocities of the stars are initially distributed according to King models, and their masses are chosen according to the Kroupa IMF (Kroupa 2001) in the range from 0.1 to $100 M_\odot$. The initial virial radius for all clusters has been selected such that the cut-off radius of the King models coincides with the cluster’s Roche, or tidal, radius, r_t , in an

external tidal Galactic field, given by

$$r_t = \left(\frac{GM_c}{2V_G^2} \right)^{1/3} R_G^{2/3} \quad (1)$$

where M_c is the total cluster mass, V_G and R_G the Galactic circular velocity and galactocentric distance, respectively. For all runs we set $V_G = 220 \text{ km s}^{-1}$, the standard value for the Milky Way. As in our previous study we included 10% hard binaries in some of our models, given their potential influence on the SBP (Vesperini & Trenti 2010) and mass segregation profile (Gill et al. 2008). Each star was tested for entry into the loss-cone, the region of angular momentum and energy space where the periapse of the stellar orbit is smaller than the tidal disruption radius of the star around the IMBH. See Umbreit et al. (2012) for a detailed description. The metallicity, Z , for the stars was set to $Z = 1 \times 10^{-3}$, and all models are evolved for 12 Gyr. We calculated the surface brightness and surface density profile by converting the stellar radius and bolometric luminosity for each star obtained from the CMC stellar evolution module BSE to V-band luminosity using the standard stellar library in Lejeune et al. (1998). Then, certain selection criteria are applied, the stellar positions projected onto the sky, and the stars binned, all in correspondence with the relevant observations (see next section). Table 1 summarizes the parameter ranges explored.

2.2. Data

We use the Milky Way GC M10 (NGC 6254) as an example for constraining the mass of a hypothetical IMBH. Here we work with the SBP from Noyola & Gebhardt (2006), taken with the WFPC2 camera on the *Hubble Space Telescope* for the inner 1.7 pc, and for the outer region with the corresponding data from the Trager catalog (Trager et al. 1995). We compare our models by, first, converting the absolute V-band luminosities of each star, we obtained as described in the previous section, to apparent magnitudes using a distance

of M10 to the sun of 4.4 kpc (Harris 1996). The stars were then projected onto the sky and binned using similar bin sizes as in Noyola & Gebhardt (2006) and Trager et al. (1995). In order to minimize the large fluctuations caused by bright giants, we impose a brightness cut-off, and only consider objects with an absolute V-band magnitude fainter than that. The cut-off is chosen as a compromise between a smooth profile and little bias in the profile shape.

Thanks to the “ACS Survey of Galactic Globular Clusters” (GO-10775; PI: A. Sarajedini) there are also deep, high-resolution observations available, with excellent photometry of main-sequence stars with masses down to $0.3 M_{\odot}$ (Beccari et al. 2010). The high resolution makes it possible to construct a sufficiently detailed star count profile, or surface density profile (SDP), for the central, denser regions of M10. For the star count profile stars were binned in concentric annuli around the center, as determined in Beccari et al. (2010). The bin widths ensure that the individual surface density values are based on at least 100 stars with the exception of the innermost bin, which contains only 38 stars. Only stars with an apparent V-band magnitude brighter than 19 are considered because, with a completeness fraction of $\approx 90\%$ (Beccari et al. 2010), they do not suffer significantly from crowding throughout the entire cluster. At a distance of 4.4 kpc from the sun and a metallicity of $Z = 0.001$ this magnitude corresponds to a main-sequence star with mass $\approx 0.7 M_{\odot}$.

Figure 1 shows the observed SBPs from Noyola & Gebhardt (2006) and the star count profile for M10. As can be seen, M10 does not possess a notable negative inner SBP or SDP slope, and Noyola & Gebhardt (2006) derive even a slightly positive value of 0.05, all not indicative of the presence of an IMBH. On the other hand, as we have shown previously (Umbreit et al. 2012), the SBP slopes are highly variable, in particular for clusters with IMBH, and therefore, the possibility remains that M10’s profile might still be consistent with

the presence of an IMBH at its center.

A simplification in choosing our initial conditions is that we only consider tidally filling clusters. However, the observed SBP cut-off radius of M10 is about 20 pc, while the tidal radius of a cluster with mass $M_c \approx 1.5 \times 10^5 M_\odot$ (McLaughlin & van der Marel 2005) at a galactocentric radius of 4.6 kpc (Harris 1996) is $r_t \approx 50$ pc. We immediately conclude that M10 is currently underfilling its Roche lobe significantly. This filling factor does not change substantially at periapse passage for an orbital eccentricity of 0.19, determined by Dinescu et al. (1999) based on an axisymmetric model for the Galactic potential. However, when the existence of bar structures in the inner ≈ 4 kpc is approximately accounted for, Allen et al. (2006) demonstrate that M10 might have experienced a much stronger tidal field at perigalacticon distances sometimes as small as 1 kpc. The large radial excursions are a direct consequence of the gravitational interactions between the cluster and the rotating bar potential, sometimes leading to the trapping of clusters in resonances and irregular orbits (Allen et al. 2006). In our study we avoid to model the complex orbit of M10, and, instead, evolve our clusters at a fixed galactocentric radius, representing an average tidal field.

3. Results

3.1. Surface Density Profile

Figure 2 shows the surface density profiles of our best fit models for M10 along with the observationally derived profile, and in Tables 2 and 3 we list their initial and final cluster parameters.

As can be seen, we are able to find models that match the surface density profile out to approximately $400''$, or 8.5 pc, for both cases, with and without IMBH. Outside of this radius, the observed profile flattens, which could be attributed to background stars or

Parameter	Range
N	$2.8 - 8 \times 10^5$
W_0	$5 - 7$
M_{BH}	$300 - 2000 M_\odot$
R_G	$0.9 - 4.1 \text{ kpc}$
Z	0.001

Table 1: Parameter ranges explored. All models were tidally filling, and their half-mass radii, thus, given by r_t from Equation 1 and W_0 , range approximately from 2 – 11 pc.

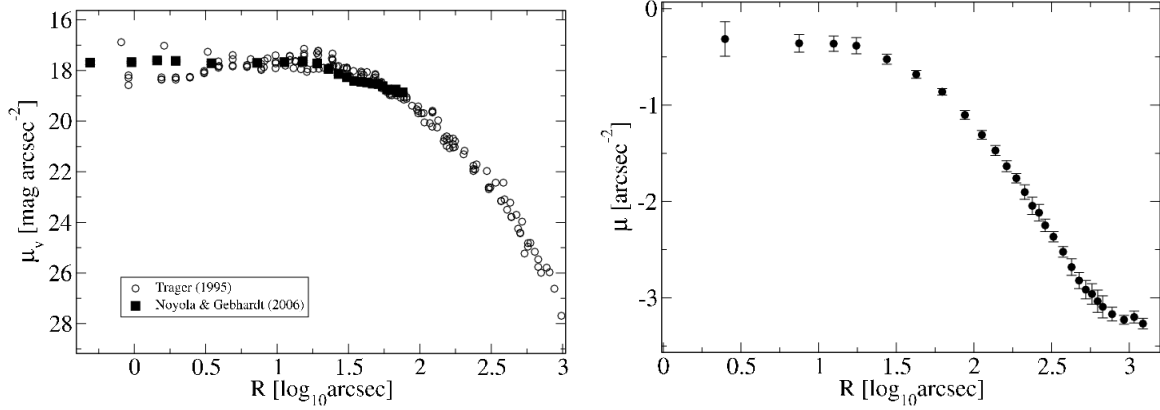


Fig. 1.— Surface brightness profile (left panel) and star count profile (right panel) of M10. The surface brightness profile combines data from Noyola & Gebhardt (2006) and Trager et al. (1995). The error bars of the star count profiles represent the Poisson error.

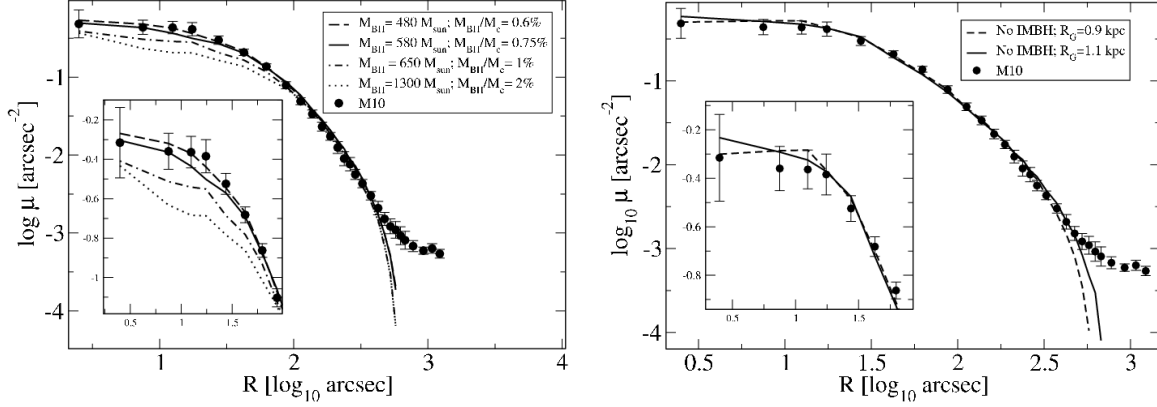


Fig. 2.— Surface density profiles from our best-fit model with (left panel) and without (right panel) a central IMBH for M10 (filled circles). Left: models with different IMBH masses at galactocentric radius of 0.9 kpc. The maximum IMBH mass for which a reasonable match to the data can be obtained is $580 M_{\odot}$. Right: Models without IMBH at 0.9 and 1.1 kpc from the Galactic center.

	$t = 0$	$t = 12 \text{ Gyr}$
N	5.0×10^5 (5.7×10^5)	1.8×10^5 (1.5×10^5)
$M_c [M_{\odot}]$	3.2×10^5 (3.6×10^5)	7.8×10^4 (6.9×10^4)
$r_h [\text{pc}]$	3.85 (3.80)	4.6 (3.90)
$t_{rh} [\text{Gyr}]$	1.6 (1.7)	4.3 (4.0)
$r_{tide} [\text{pc}]$	25.8 (23.5)	16.0 (13.6)

Table 2: Evolution of the characteristics of our best-fit models without IMBH. Shown are the parameters for the model with $R_G = 1.1 \text{ kpc}$ and, in parentheses, for the model with $R_G = 0.9 \text{ kpc}$. Here, r_h is the half-mass radius, r_t the tidal, or Jacobi, radius, and M_c the total cluster mass.

escaping stars that remain still close to the cluster. This could be due to the significant non-sphericity of the combined cluster and Galactic potential (Fukushige & Heggie 2000; Küpper et al. 2010), which cannot be modeled with the simple tidal cut-off prescription used in our code (see Chatterjee et al. 2010). Given the rather large core to half-light ratio of M10 of ≈ 0.4 (Harris 1996), it is not surprising that the models without IMBH are still in the core contracting phase. This is also shown in Figure 3, where the evolution of the corresponding core-to-half-mass ratio is shown. It should be noted here that the core radius in this figure is calculated from both stars and stellar remnants, and, due to the strong concentration of the dark remnants towards the cluster center, has a significantly smaller value at the end of the simulation.

From Figure 2 we also see that M10 can only harbor an IMBH with at most $580 M_{\odot}$. Given the low final mass of the clusters of $\approx 8 \times 10^4 M_{\odot}$, this corresponds to a BH-to-cluster mass ratio of 0.75%, much larger than what we would expect from the extrapolated $M_{BH} - \sigma$ relation (Ferrarese & Merritt 2000; van der Marel 2001; Kormendy & Richstone 1995). However, the main reason for the large value is that the cluster lost 80% of its initial mass, while initially the BH-to-cluster mass ratio was 0.15%, in good agreement with the $M_{BH} - \sigma$ relation.

3.2. Surface Brightness Profile

An alternative method to detect imprints of an IMBH is to construct the SBP from integrated light measurements. The advantages and disadvantages of integrated light profiles with respect to star count profiles have been discussed by Noyola & Gebhardt (2006) and Noyola & Baumgardt (2011). In short, star count profiles suffer from crowding, whereby faint stars cannot be detected in the vicinity of bright stars affecting the overall profile shape. Therefore, star count profiles are usually limited to fewer, brighter stars

	$t = 0$	$t = 12 \text{ Gyr}$
N	5.7×10^5	1.7×10^5
$M_c \text{ [M}_\odot\text{]}$	3.6×10^5	7.7×10^4
$r_h \text{ [pc]}$	3.4	4.1
$t_{rh} \text{ [Gyr]}$	1.5	4.1
$r_{tide} \text{ [pc]}$	23.5	14.0

Table 3: Evolution of the characteristics of our best-fit models with IMBH. Shown are the parameters for the model with a final $M_{BH} = 480 \text{ M}_\odot$, and $R_G = 0.9 \text{ kpc}$.

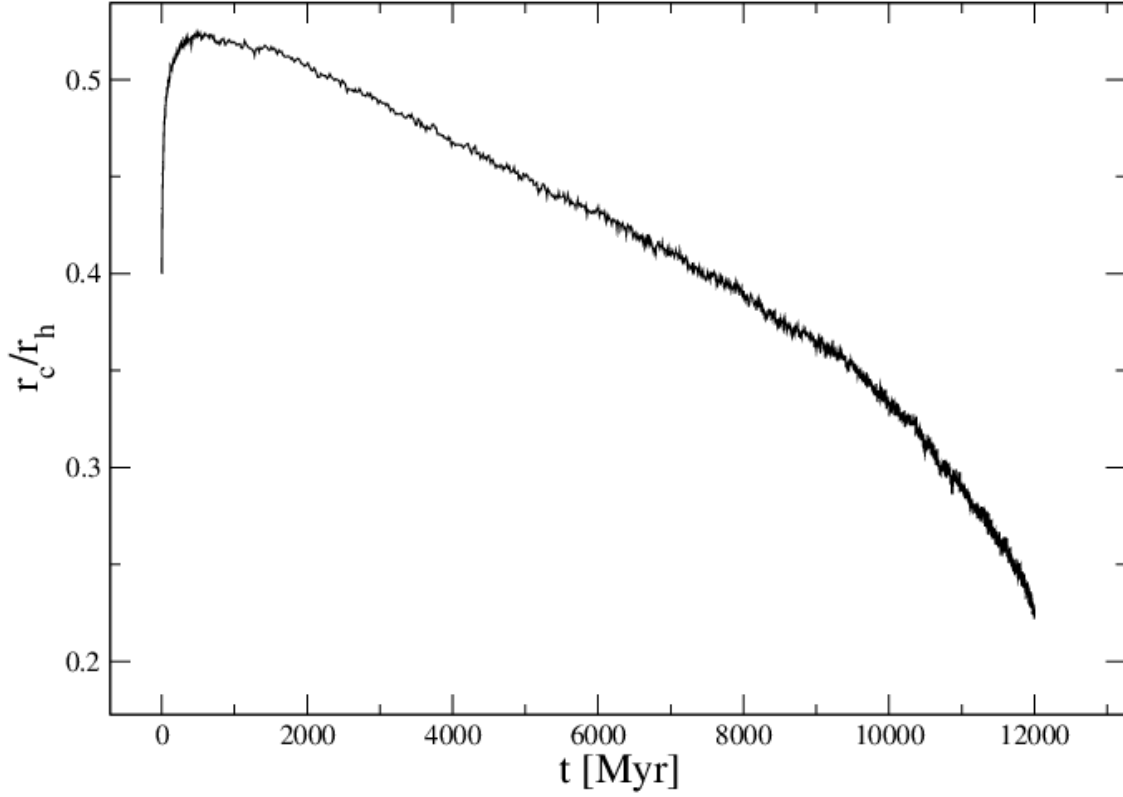


Fig. 3.— Core-to-half-mass radius over time for the best-fit model without IMBH at $R_G = 0.9 \text{ kpc}$.

with high completeness, which in turn, however, makes the profiles noisier. In contrast, integrated light profiles contain the contribution of all stars, but a few very bright giants can contribute disproportionately to it, resulting in larger noise levels. The brightest stars are, therefore, removed before the profile is calculated. In real images this subtraction cannot be done cleanly and there is always a hard-to-quantify contribution from the wings of the point-spread-function of subtracted giants (Noyola & Gebhardt 2006). An accurate comparison to theoretical models, thus, would require producing synthetic images from the models and repeating exactly the same procedure that has been done to derive the observed profile, as has been carried out in Noyola & Baumgardt (2011). Here, we chose instead a simpler procedure by removing all stars above a certain cut-off magnitude with a value chosen as a compromise between low noise levels and minimal changes in the profile shape.

Figure 4 shows the SBP of the best-fit M10 model from the previous section with $R_G = 0.9$ kpc, applying two cut-off magnitudes to mask bright giants. As can be seen, the model SBP follows the observed profile well, and, therefore, the observed surface brightness and the star count data, despite being derived from rather different observations, and possibly constructed relative to different cluster centers, appear to be consistent with each other. However, in contrast to our previous models for NGC 5694, the influence of the absolute cut-off magnitude is profound, and giants up to an absolute magnitude of -0.5 mag contribute significantly to the total cluster light throughout. The reason for this could be related to the strong tidal stripping that led, together with the mass lost from stellar evolution, to about 80% mass loss for our model clusters at the end of the simulations. Since preferentially low-mass stars are removed through this process, the low-mass end of the mass function flattens (e.g., Baumgardt & Makino 2003), and the brighter, more massive giants contribute more to the total cluster light. Clearly, a simple cut-off prescription in absolute magnitude is, in this case, not sufficient to obtain a smooth profile and match the observed profile. This limits the extent to which we can put constraints on the IMBH mass.

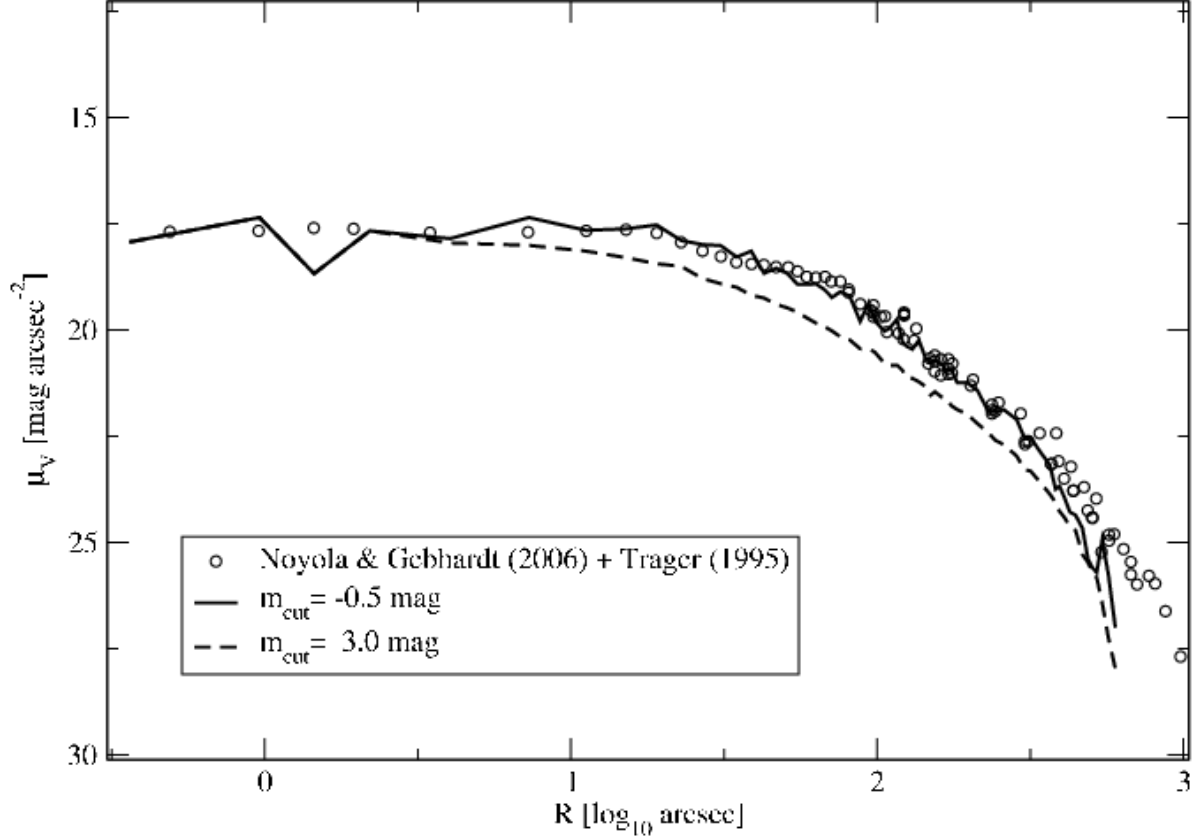


Fig. 4.— Surface brightness profile for the best fit model without IMBH. Shown is the combined observed profile (open circles) from Noyola & Gebhardt (2006) and Trager et al. (1995) (inside and outside 76 arcsec respectively), as well as the profile of our best fit model with $R_G = 0.9$ kpc and two absolute cut-off V-band magnitudes, 3 mag (dashed line) and -0.5 mag (solid line), for the masking of bright giants. The model SBP follows the observed profile well and both, observed SBP and SDP, are, thus, consistent with each other. The influence of the cut-off magnitude on the SBP is, with ≈ 1 mag difference in the profiles, significant and much larger than for the models in Umbreit et al. (2012) (< 0.2 mag for the same cut-off values).

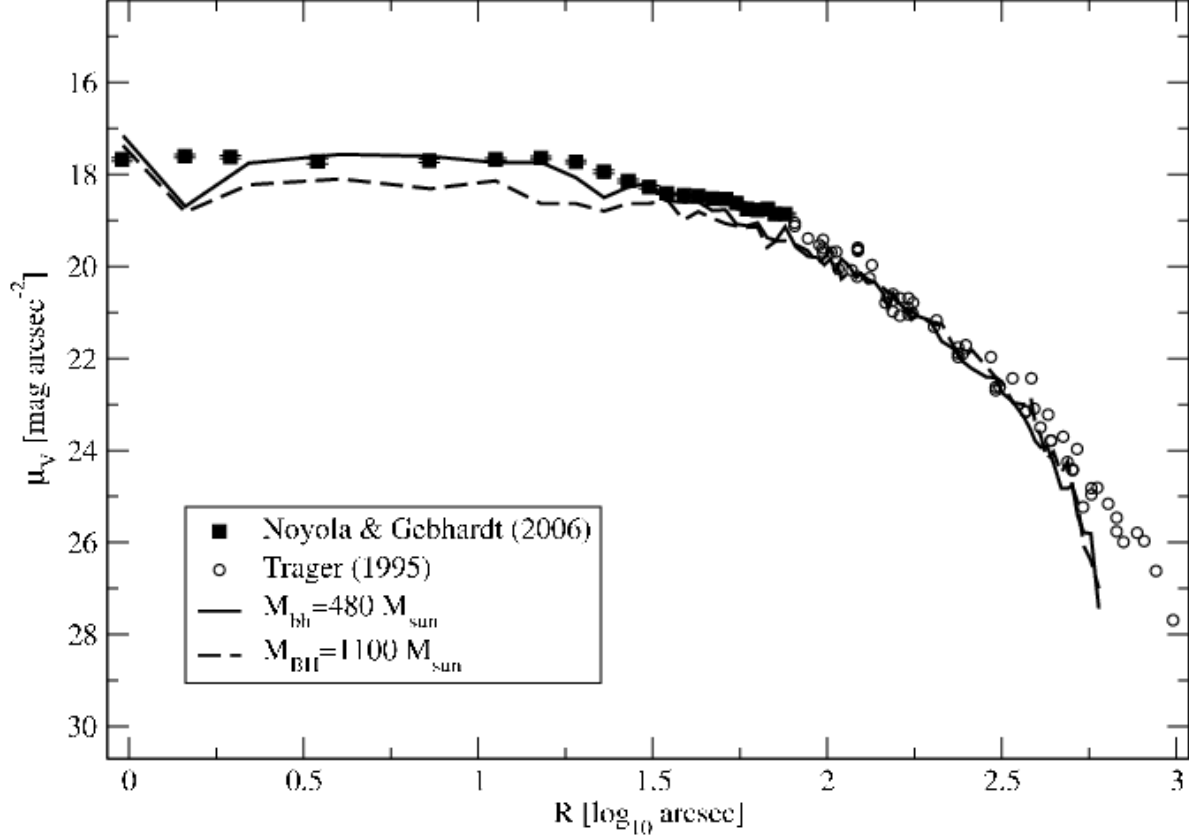


Fig. 5.— Surface brightness profiles of models with an IMBH. Shown here are the observed profiles of Noyola & Gebhardt (2006) (filled squares) and Trager et al. (1995) (open circles) and two model profiles with IMBH masses of $480 M_{\odot}$ (solid line) and $1100 M_{\odot}$ (dashed lines). The $480 M_{\odot}$ IMBH model is the same as in Fig. 2. Due to the noise in the profiles, caused by very bright giants, it is difficult to discern models with a difference in IMBH mass of less than $500 M_{\odot}$.

Figure 5 shows our results for models with IMBH. Both models have the same initial conditions as in Figure 4 and only differed in IMBH mass. As can be seen, the model with $M_{BH} = 480 M_{\odot}$, which is the same as the one in the previous section, fits the observed profile reasonably well. However, because of the noise in the profile, only a model with $M_{BH} = 1100 M_{\odot}$ can be clearly ruled out, while models with smaller M_{BH} are harder to distinguish. A smoother profile is generally more desirable as it allows stronger constraints to be placed on the mass of a hypothetical central IMBH. More sophisticated and elaborate techniques, as, e.g., presented in Noyola & Baumgardt (2011), are necessary for this purpose.

3.3. Mass Segregation

A more recently proposed diagnostic for the presence of an IMBH in a GC (Gill et al. 2008), is based on the tendency for mass segregation to be suppressed by strong interactions in the vicinity of a central IMBH. The signature is, however, not unique, as binary interactions lead to a similar decrease in the average mass provided the binaries are sufficiently numerous and hard. Beccari et al. (2010) determined through deep photometry with the ACS camera on *HST* the mean mass profile for M10, which is defined as (Pasquato et al. 2009)

$$\Delta m(r) = \langle m \rangle(r) - \langle m \rangle(r_h)$$

where $\langle m \rangle(r)$ is the mean stellar mass at distance r from the cluster center, and r_h the half-mass radius. They found that both a cluster with an IMBH, or a cluster without IMBH but with a binary fraction $> 5\%$, can reproduce the observed profile. In an effort to draw firmer conclusions as to whether an IMBH is required to explain the mean mass profile in M10, Dalessandro et al. (2011) compared the observed radial dependence of the binary fraction with the corresponding results of the simulations in Beccari et al. (2010) and

found that the observed fractions are always larger than in the models with a global binary fraction of 5%. They conclude that the binary fraction is large enough to suppress mass segregation in the center of M10 and an IMBH is not needed to explain the observations.

The mass segregation signature, however, develops only after the cluster has had enough time to relax, typically $\sim 5 t_{rh}$ (Gill et al. 2008). From Tables 2 and 3 we already see that the half-mass relaxation times in our models are rather large and vary by a factor of more than two during the cluster evolution, which makes it not so clear whether M10 is really old enough for the mass segregation signature to be discernible. To address this issue, we analyze our best fit models following the same procedure used for the N -body models in Beccari et al. (2010), and compare to the corresponding observations.

Figure 6 shows the mean mass profile of M10 and our best fit cluster models with and without IMBH, including models with 10% and 0% binaries. As can be seen, all model profiles match the data in Beccari et al. (2010) very closely, which is somewhat surprising given that we would expect the model with no binaries and no IMBH to be more strongly segregated than the others. The differences, instead, are rather marginal, which could indeed indicate that M10 is still dynamically young. When we calculate the dynamical age as the number of elapsed half-mass relaxation times, $N_{t_{rh}}$, defined by Hurley (2007) as

$$N_{t_{rh}} = \int_0^\tau \frac{dt}{t_{rh}(t)} \quad (2)$$

where τ is the cluster age, we obtain $N_{t_{rh}} = 2.6, 2.4, 2.8$ for the single star, binary and IMBH cluster models, respectively. Thus, compared, e.g., to NGC 5694 (Umbreit et al. 2012), M10 appears to be dynamically only half as old. As can be seen in Figures 2 and 3 in Gill et al. (2008), at these young ages the innermost points, $\Delta m(0)$, still overlap significantly between the different models, making it difficult, if not impossible, to discern between clusters with and without IMBH. In order to illustrate this point further, we also calculated $\Delta m(r)$ for dynamically more evolved clusters, with a larger initial concentration

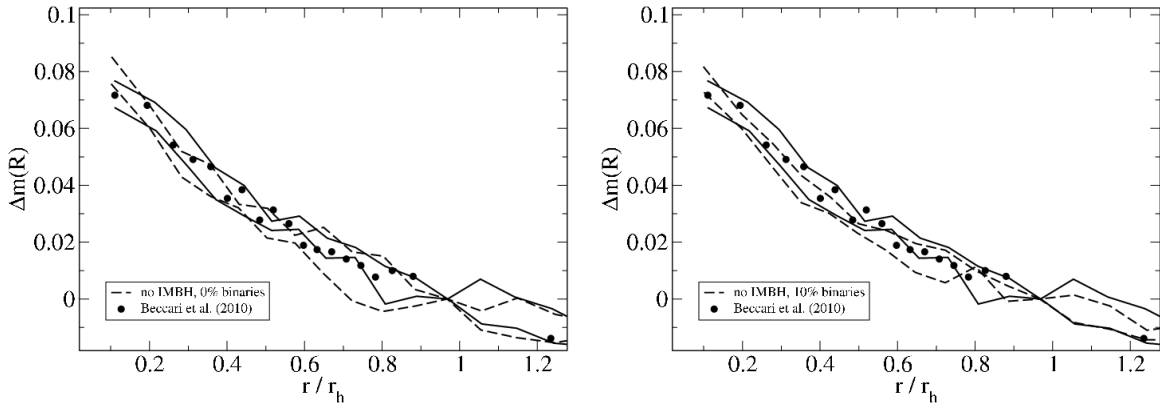


Fig. 6.— Average mass profile for our best-fit models with and without IMBH. Each final cluster state was projected on the sky from 10 random directions, and shown are two of the resulting profiles that roughly embrace all the others. Left: Results with and without IMBH and no binaries. Right: Results with and without IMBH and 10% hard binaries. All models reproduce the average mass profile very well, and there are only negligible differences between them. The reason is most likely the young dynamical age of M10, as only little more than two half-mass relaxation times have elapsed.

($W_0 = 7$ instead of $W_0 = 5.6$) but otherwise the same initial conditions as our best fit clusters. As Figure 7 shows, the clusters without IMBH now have a clearly larger average stellar mass at the center, while the model with IMBH has an average mass profile that is very similar to the one in Figure 6. This clearly confirms that our best fit models without IMBH have not yet reached their fully relaxed state, and the reason for the lower level of mass segregation in M10 could simply be a consequence of its young dynamical age, rather than the presence of a IMBH in its center.

3.4. Velocity Dispersion

One of the great advantages of modeling the evolution of clusters on a star-by-star basis with the full number of stars is that the resulting models allow us to make detailed predictions for observations. This is especially important for the detection of the velocity dispersion signature of IMBHs, as for the expected IMBH masses, the radial extent of the inner cusp is small and does not contain many objects (Baumgardt et al. 2004a), making the interpretation of the data very challenging. The problem becomes even more severe considering that, through mass segregation, the center of the cluster is dominated by dark remnants, further reducing the number of bright stars available for velocity measurements in the cusp. Here we determine to what extent we can expect to detect an increase in velocity dispersion for the innermost bright stars in the core of M10.

In Figure 8 we show the projected one-dimensional velocity profile of our model with $M_{\text{BH}} = 480 M_{\odot}$ including only bright main-sequence stars and giants above certain brightness cut-offs. Each point in this profile represents the velocity dispersion of 20 neighboring stars.

As can be seen, the velocity dispersion cusp extends out to $\approx 3''$ and contains in each

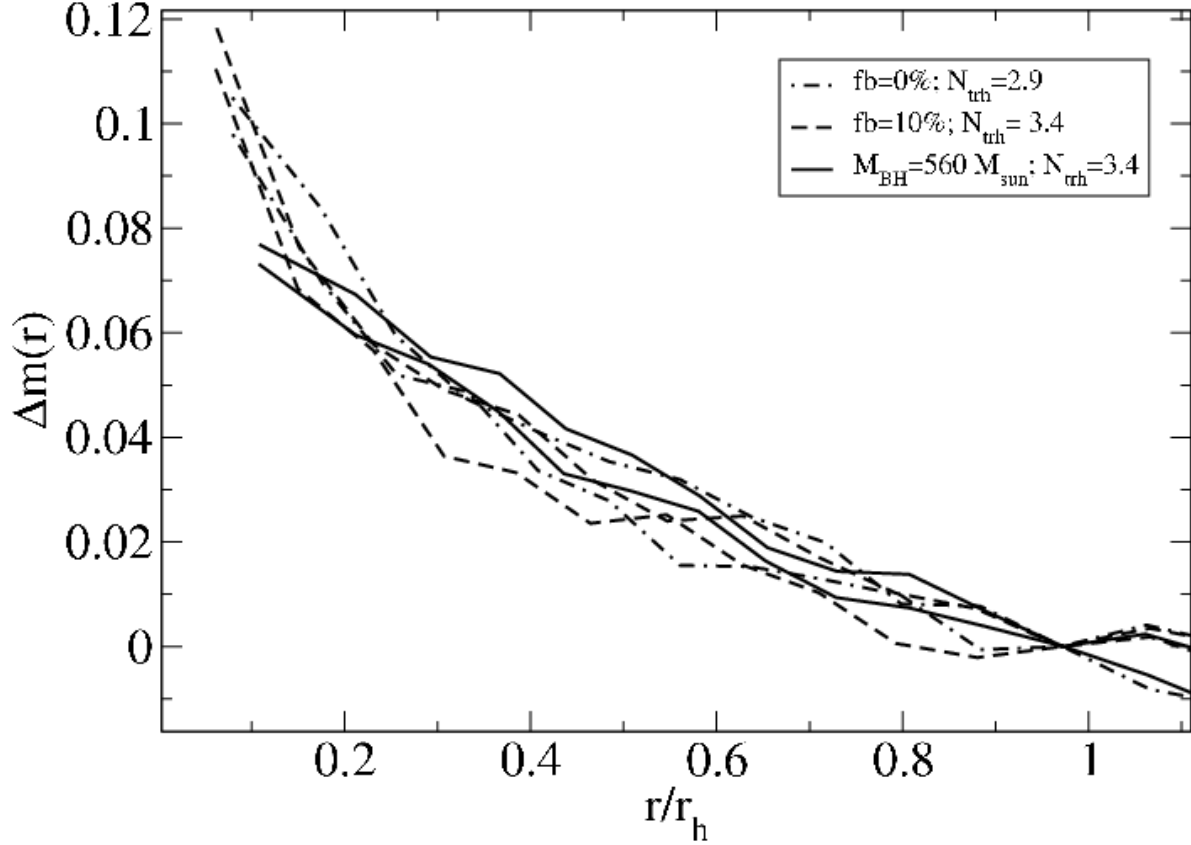


Fig. 7.— Mean mass profile for more evolved clusters. All models have initial conditions as in Table 2 and 3 but started more concentrated, making them dynamically more evolved at 12 Gyr. While there is little change compared to Fig. 6 for the model with IMBH, the models without IMBH show a significantly increased level of mass segregation in the center.

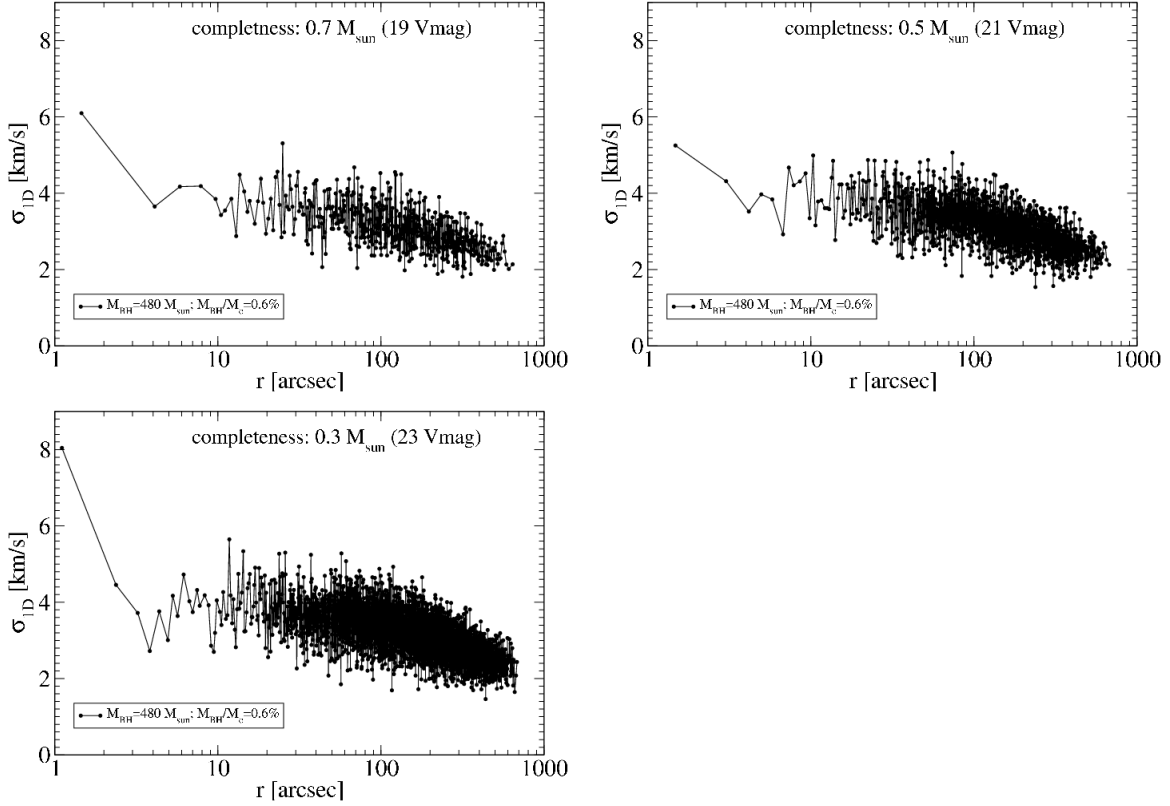


Fig. 8.— Projected one-dimensional velocity dispersion profile of our best fit model with $M_{BH} = 480 M_{\odot}$, for various completeness levels. Each point represents the velocity dispersion of 20 stars. The scatter of the values is of the order of the Poisson error, and is about 1 km s^{-1} . A cusp with an extension of $3''$ is visible, but contains only 20 – 40 stars. A significant increase in velocity dispersion is only detectable if also low-mass stars, with masses down to $0.3 M_{\odot}$, are considered.

case 20 – 40 bright stars. Furthermore, the velocity dispersion of the innermost point is only about 50% larger than the average in the cluster core, even when the completeness limit is as low as $0.5 M_{\odot}$. Given that the statistical fluctuation of each point, as determined from 10 random projections of the cluster on the sky, is $\approx 2 \text{ km s}^{-1}$, this increase is barely significant. Only for a limit of $0.3 M_{\odot}$ does the velocity dispersion of the innermost point become significantly larger, and, with twice the value, can be clearly distinguished from the core velocity dispersion. The reason for the increase in velocity dispersion with decreasing brightness cut-off is that, as more stars are included, the first 20 stars sample a region closer to the IMBH, where velocities are larger.

From this we can see that detecting an IMBH with only about $500 M_{\odot}$ in M10 based on velocity dispersion measurements alone is extremely challenging and would require very deep observations with completeness limits down to $0.3 M_{\odot}$. This is despite the fact that the radial extent of the cusp, out to about $3''$, is large enough to be easily resolved. The sparseness of bright stars in the central region prevents sampling the velocity dispersion close enough to the IMBH to detect a significantly increase above the core velocity dispersion.

4. Summary and Conclusions

We carried out Monte Carlo simulations to constrain IMBHs at the centers of observed GCs considering a variety of observational diagnostics. In contrast to our earlier study (Umbreit et al. 2012), we focused on a cluster, M10, that undergoes significant tidal stripping, resulting in final cluster masses of only about 20% of the initial.

From a comparison to a detailed star count profile we were able to put an upper limit on the mass of a hypothetical IMBH in M10. We find that the maximum IMBH mass that

results in a SDP that still fits the observed profile is $\approx 600 M_{\odot}$. This IMBH mass also leads to a SBP that is compatible with observations by Noyola & Gebhardt (2006), although due to the large radial fluctuations caused by very bright giants, the SBP is less constraining. This is in contrast to our earlier investigation of the cluster NGC 5694 (Umbreit et al. 2012) where the SBP was much less noisy. The reason is mostly likely that the light in M10 is dominated by bright giants as we find that the model profile shape is rather sensitive to the chosen cut-off brightness. This could be a direct consequence of the preferential loss of low-mass stars through tidal stripping, which causes the low-mass end of the mass function to flatten, and the brighter, more massive giants contribute more to the total cluster light. The more detailed analysis in Noyola & Baumgardt (2011) might lead to a much smoother profile, and, therefore, could have the potential to obtain stronger constraints for an IMBH in M10 than star count data, as integrated light measurements generally include the contribution of many more stars.

In addition to light and star count profiles, we also considered the amount of mass segregation in M10 as an indicator of an IMBH. Our main finding is that M10 is not dynamically relaxed enough for the IMBH signature, a relative depression of the mean stellar mass at the cluster center, to be detectable. Indeed, when calculating the number of elapsed half-mass relaxation times (Equation 2), M10 is dynamically only half as old as NGC 5694 and still in its core contraction phase. Similar to the case of NGC 5694 in Umbreit et al. (2012), this demonstrates that simple dynamical age estimates based on the current state of globular cluster are extremely uncertain. We also showed that interactions of stellar binaries are not able to sustain the large core of M10 ($r_c/r_h \approx 0.4$; Harris 1996) even with a binary fraction as large as 10%.

Finally, we found that the velocity dispersion signature of an IMBH in our best-fit M10 model is very challenging to detect. This is because the Keplerian cusp is rather sparsely

populated with bright stars and main-sequence stars with masses down to $0.3 M_{\odot}$ have to be included in a future velocity measurement in order to detect a significant increase for the innermost 20-40 stars. Given that $0.3 M_{\odot}$ stars have been detected with only a 50% completeness in the core of M10 by Beccari et al. (2010), detecting such an increase remains difficult even when a second epoch of ACS data with a sufficiently long time baseline becomes available.

We thank Barbara Lanzoni for providing us with the star count data for M10 from HST archival data (GO-10775; PI: A. Sarajedini). S.U. was supported by Hubble Theory Program HST-AR-11779, provided by NASA through a grant from the Space Telescope Science Institute, which is operated by the Association of Universities for Research in Astronomy, Inc., under NASA contract NAS 5-26555. We also acknowledge support from NASA ATP Grant NNX09AO36G at Northwestern University. This work was started while the authors and Barbara Lanzoni were participants of the program “Formation and Evolution of Globular Clusters” at KITP in Spring 2009. Our work at KITP was supported in part by the National Science Foundation under Grant No. NSF PHY11-25915.

REFERENCES

- Aarseth, S. J. 2003, *Gravitational N-Body Simulations*, ed. S. J. Aarseth
- Allen, C., Moreno, E., & Pichardo, B. 2006, *ApJ*, 652, 1150
- Baumgardt, H. & Makino, J. 2003, *MNRAS*, 340, 227
- Baumgardt, H., Makino, J., & Ebisuzaki, T. 2004a, *ApJ*, 613, 1133
- . 2004b, *ApJ*, 613, 1143
- Baumgardt, H., Makino, J., & Hut, P. 2005, *ApJ*, 620, 238
- Beccari, G., Pasquato, M., De Marchi, G., Dalessandro, E., Trenti, M., & Gill, M. 2010, *ApJ*, 713, 194
- Bettwieser, E. & Sugimoto, D. 1984, *MNRAS*, 208, 493
- Chatterjee, S., Fregeau, J. M., & Rasio, F. A. 2008, in *IAU Symposium*, Vol. 246, IAU Symposium, 151–155
- Chatterjee, S., Fregeau, J. M., Umbreit, S., & Rasio, F. A. 2010, *ApJ*, 719, 915
- Dalessandro, E., Lanzoni, B., Beccari, G., Sollima, A., Ferraro, F. R., & Pasquato, M. 2011, *ApJ*, 743, 11
- Dinescu, D. I., Girard, T. M., & van Altena, W. F. 1999, *AJ*, 117, 1792
- Ferrarese, L. & Merritt, D. 2000, *ApJ*, 539, L9
- Fregeau, J. M., Gürkan, M. A., Joshi, K. J., & Rasio, F. A. 2003, *ApJ*, 593, 772
- Fregeau, J. M. & Rasio, F. A. 2007, *ApJ*, 658, 1047
- Fukushige, T. & Heggie, D. C. 2000, *MNRAS*, 318, 753

- Gill, M., Trenti, M., Miller, M. C., van der Marel, R., Hamilton, D., & Stiavelli, M. 2008, *ApJ*, 686, 303
- Harris, W. E. 1996, *AJ*, 112, 1487
- Heggie, D. C., Hut, P., Mineshige, S., Makino, J., & Baumgardt, H. 2007, *PASJ*, 59, L11
- Hurley, J. R. 2007, *MNRAS*, 379, 93
- Joshi, K. J., Nave, C. P., & Rasio, F. A. 2001, *ApJ*, 550, 691
- Joshi, K. J., Rasio, F. A., & Portegies Zwart, S. 2000, *ApJ*, 540, 969
- Kormendy, J. & Richstone, D. 1995, *ARA&A*, 33, 581
- Kroupa, P. 2001, *MNRAS*, 322, 231
- Kruijssen, J. M. D., Pelupessy, F. I., Lamers, H. J. G. L. M., Portegies Zwart, S. F., & Icke, V. 2011, *MNRAS*, 414, 1339
- Küpper, A. H. W., Kroupa, P., Baumgardt, H., & Heggie, D. C. 2010, *MNRAS*, 407, 2241
- Lejeune, T., Cuisinier, F., & Buser, R. 1998, *A&AS*, 130, 65
- Marchant, A. B. & Shapiro, S. L. 1980, *ApJ*, 239, 685
- McLaughlin, D. E. & van der Marel, R. P. 2005, *ApJS*, 161, 304
- Miocchi, P. 2007, *MNRAS*, 381, 103
- Noyola, E. & Baumgardt, H. 2011, *ApJ*, 743, 52
- Noyola, E. & Gebhardt, K. 2006, *AJ*, 132, 447
- Pasquato, M., Trenti, M., De Marchi, G., Gill, M., Hamilton, D. P., Miller, M. C., Stiavelli, M., & van der Marel, R. P. 2009, *ApJ*, 699, 1511

- Portegies Zwart, S. F., McMillan, S. L. W., Hut, P., & Makino, J. 2001, MNRAS, 321, 199
- Shapiro, S. L. 1977, ApJ, 217, 281
- Trager, S. C., King, I. R., & Djorgovski, S. 1995, AJ, 109, 218
- Trenti, M., Ardi, E., Mineshige, S., & Hut, P. 2007, MNRAS, 374, 857
- Trenti, M., Vesperini, E., & Pasquato, M. 2010, ApJ, 708, 1598
- Umbreit, S., Fregeau, J. M., Chatterjee, S., & Rasio, F. A. 2012, ApJ, 750, 31
- van der Marel, R. P. 2001, in Black Holes in Binaries and Galactic Nuclei, ed. L. Kaper, E. P. J. V. D. Heuvel, & P. A. Woudt, 246
- Vesperini, E. & Trenti, M. 2010, ApJ, 720, L179
- Wyller, A. A. 1970, ApJ, 160, 443